Mon. Not. R. Astron. Soc. **344,** 1029–1040 (2003)

Strong lensing constraints on the velocity dispersion and density profile of elliptical galaxies

Adam N. Davis,[1] Dragan Huterer[1★] and Lawrence M. Krauss[1,2]

[1]*Department of Physics, Case Western Reserve University, Cleveland, OH 44106, USA*
[2]*Department of Astronomy, Case Western Reserve University, Cleveland, OH 44106, USA*

Accepted 2003 May 5. Received 2003 March 17; in original form 2002 October 24

ABSTRACT

We use the statistics of strong gravitational lensing from the Cosmic Lens All-Sky Survey to impose constraints on the velocity dispersion and density profile of elliptical galaxies. This approach differs from much recent work, where the luminosity function, velocity dispersion and density profile have been typically *assumed* in order to constrain cosmological parameters. It is indeed remarkable that observational cosmology has reached the point where we can consider using cosmology to constrain astrophysics, rather than vice versa. We use two different observables to obtain our constraints: total optical depth and angular distributions of lensing events. In spite of the relatively poor statistics and the uncertain identification of lenses in the survey, we obtain interesting constraints on the velocity dispersion and density profiles of elliptical galaxies. For example, assuming the singular isothermal sphere density profile and marginalizing over other relevant parameters, we find $168 \leqslant \sigma_* \leqslant 200$ km s^{-1} (68 per cent confidence level), and $158 \leqslant \sigma_* \leqslant 220$ km s^{-1} (95 per cent confidence level). Furthermore, if we instead assume a generalized Navarro–Frenk–White density profile and marginalize over other parameters, the slope of the profile is constrained to be $1.50 \leqslant \beta \leqslant 2.00$ (95 per cent confidence level). We also constrain the concentration parameter as a function of the density profile slope in these models. These results are essentially independent of the exact knowledge of cosmology. We briefly discuss the possible impact on these constraints of allowing the galaxy luminosity function to evolve with redshift, and also possible useful future directions for exploration.

Key words: gravitational lensing – galaxies: elliptical and lenticular, cD – galaxies: structure.

1 INTRODUCTION

The statistics of strong gravitational lensing has repeatedly been advertised and used as a probe of cosmology (Turner, Ostriker & Gott 1984; Hinshaw & Krauss 1987; Fukugita et al. 1992; Krauss & White 1992; Kochanek 1995, 1996; Cooray, Quashnock & Miller 1999; Chiba & Yoshii 1999; Cheng & Krauss 1999). The sensitivity of lensing counts to $\Omega_{\rm M}$ and Ω_Λ, the energy densities in matter and the vacuum component relative to the critical, comes mostly from a volume effect; higher Ω_Λ implies bigger comoving volume for a fixed redshift, leading to the higher optical depth for lensing. Using knowledge about the luminosity function of galaxies and their density profiles, many authors have used lensing statistics to constrain cosmological parameters. For example, Fukugita & Turner (1991) first constrained the vacuum energy density to be less than about 90 per cent of the critical energy density ($\Omega_\Lambda \lesssim 0.9$) at 95 per cent confidence level (hereafter CL). Subsequently, this was followed by Kochanek (1995, 1996), who claimed an upper limit on the vacuum energy density ($\Omega_\Lambda < 0.66$ at 95 per cent CL). Krauss & White (1992) and later Chiba & Yoshii (1999) and Cheng & Krauss (1999) used a different choice of galaxy parameters and demonstrated that a flat vacuum-energy-dominated universe could be favoured. Similar analyses have been performed by Im, Griffiths & Ratnatunga (1997), Cooray et al. (1999), Waga & Miceli (1999), and all typically favour the Λ cold dark matter (CDM) cosmology. Cheng & Krauss (1999, 2001) also explored how uncertainties in the choice of galaxy parameters could result in vastly different constraints on cosmology, although they argued for a choice that ultimately favoured a flat, vacuum-energy-dominated cosmology. It has also recently been argued that strong lensing statistics from ongoing surveys such as the Sloan Digital Sky Survey (SDSS) might impose interesting constraints on the equation-of-state ratio of dark energy w (Cooray & Huterer 1999); constraints on w from lensing have already been claimed by Sarbu, Rusin & Ma (2001) who used the statistics of the Jodrell Very Large Array Astrometric Survey/Cosmic Lens All-Sky Survey (JVAS/CLASS) to obtain $w \lesssim -0.4$. Similar results have been obtained very recently by Chae et al. (2002).

★E-mail: dhuterer@bombur.phys.cwru.edu

Given the notoriously poor statistics of strong lensing surveys thus far – the total number of gravitational lenses is of the order of 50, and the largest homogeneous survey (which we use in this work), JVAS/CLASS, currently has a total of only 17 events – combined with the existing galactic luminosity function uncertainties, it is not clear how seriously we should take any constraints on cosmology derived from strong lensing statistics. To constrain cosmological parameters using lensing statistics, we have to deal with the strong dependence of the results on the lens profile, the density dispersion of galactic dark matter, the number density of galaxies as a function of redshift, and observational effects due to magnification bias and the selection function of the survey.

In this work, we exploit this sensitivity to reverse the traditional methodology. Because lensing statistics are, on the whole, much more sensitive to astrophysical than cosmological parameters, we wish to utilize existing surveys to probe the properties of lensing galaxies rather than cosmology. We are aided in this effort at this time because independent probes of cosmological parameters have recently converged rather tightly on a single cosmological model: a flat dark energy dominated universe with $\Omega_{\rm DE} \approx 0.7$, and $\Omega_{\rm M} \approx 0.3$. As these parameters currently seem to be more tightly constrained than the galaxy parameters described above, now seems an opportune time to use cosmology to constrain astrophysics, rather than vice versa!

Some efforts along these lines have already been explored, as new and better lensing data, especially the JVAS/CLASS, have appeared. In particular, several investigations have been undertaken to constrain the nature of galaxy clustering in the CDM paradigm. Keeton (2001) used the statistics of JVAS/CLASS lenses to indicate that CDM galaxies are too concentrated to agree with the lensing statistics, while Keeton & Madau (2001) used the absence of wide-separation lenses in the CLASS to impose an upper bound on the concentration of dark matter haloes. Takahashi & Chiba (2001) have considered lensing by both singular isothermal sphere (SIS) and Navarro–Frenk–White (NFW) profile galaxies, and have found that the lack of observed large-angle separation lenses indicates that the density profile is not too steep ($\beta \lesssim 1.5$, with $\rho(r) \propto r^{-\beta}$). Oguri, Taruya & Suto (2001) have obtained a similar result by using the statistics of tangential and radial arcs. Conversely, Rusin & Ma (2001) used the absence of detectable odd images to set a constraint on the surface density of lensing galaxies, and concluded that lenses cannot have profiles much shallower than a SIS ($\beta \gtrsim 1.8$). Wyithe, Turner & Spergel (2001) and Li & Ostriker (2002) considered lensing by objects with both SIS and generalized NFW (GNFW) density profiles. They computed optical depths, image separations and magnification biases. In particular, Li & Ostriker, extending the earlier work of Keeton (1998) and Porciani & Madau (2000) argued that, in order to explain the large number of observed small-separation lenses and the lack of large-separation events (compared to predicted distributions for lensing by clusters), the favoured galaxy cluster profile seems to be the combination of SIS (when $M \lesssim 10^{13}$ M$_{\odot}$) and NFW (when $M \gtrsim 10^{13}$ M$_{\odot}$).

Here we carry out a related analysis, with the aim of constraining the nature of individual galaxies rather than clusters. For this purpose we shall assume the 'concordance' values for the cosmological parameters (e.g. Krauss 2000) – $\Omega_{\rm M} = 1 - \Omega_{\rm DE} = 0.3$, $w = -1$ and $h = 0.7$ – where $\Omega_{\rm M}$ and $\Omega_{\rm DE}$ are energy densities in matter and dark energy relative to critical, w is the equation of state ratio of dark energy, and $H_0 = 100\, h$ km s^{-1} Mpc^{-1}. We will show that our results are extremely weakly dependent on the assumed cosmology (in particular, knowledge of $\Omega_{\rm M}$).

2 THE DATA

Although more than 60 multiply imaged quasars and radio sources are known, they come from different observations with different sensitivities and selection functions, which makes an accurate computation of the expected number of lenses very difficult. Therefore, it is imperative to have data from a single well-understood survey with information on the source population. In this work, we use the most complete homogeneous sample of lenses provided by the CLASS (Myers et al. 2003; Browne et al. 2003), which extended the earlier JVAS (Patnaik et al. 1992a; King et al. 1999). The CLASS uses the Very Large Array to image radio sources with the flux density of between 30 and 200 mJy; candidate lensing events are followed up by Multi-Element Radio-Linked Interferometer Network (MERLIN) and the National Radio Astronomy Observatories (NRAO) Very Large Baseline Array (VLBI). So far, a total of about 16 000 sources have been imaged by JVAS/CLASS, with 22 confirmed lensing events. Of these, a subset of 8958 sources with 13 lenses forms a well-defined subsample suitable for statistical analysis (Browne et al. 2003), and we use this subsample in our work. Table 1, essentially identical to table 3 in Browne et al. (2003), shows the lenses from the statistically controlled subsample. We have added information about the identity of the lens, in particular whether it is a spiral galaxy, an elliptical, or formed by more than one galaxy (Chae 2003).

It is well known that elliptical galaxies dominate the optical depth for strong lensing by individual galaxies (e.g. Kochanek 1993b), and as a result we concentrate on constraining their parameters here. This effort is complicated by the fact that only six of the CLASS lenses are clearly identified as ellipticals and one as a spiral, while in other cases the identity of the lens is uncertain; see Table 1. Furthermore, three events are due to more than one lens galaxy. It is crucial to choose a subset of CLASS lenses that includes elliptical galaxies only. It is clear that the number of ellipticals is between 6 and 12, and that confirmed ellipticals outnumber spirals in the ratio 6:1. The most likely value of the number of ellipticals is therefore somewhere near 11. To compute the measured number of lenses, we chose to marginalize over the range between 6 and 12, with the Gaussian weighting centred at 11 and a variance of 5. However, as we later discuss, the results are extremely insensitive to the exact choice of weighting; the reason is that the statistics are much more sensitive to the parameters we wish to constrain – the velocity dispersion and density profile of elliptical galaxies. For the angular separation test, we use only the four *single*[1] elliptical lenses (B0712+472, B1422+231, B1933+503, B2319+051). To test the robustness of this test, we alternatively assume that all unidentified galaxies are ellipticals as well, and use a total of nine *single* non-spiral lenses (the four above, plus B0445+123, B0631+519, B0850+054, B1152+199 and B2045+265). As discussed later, our results are insensitive to the exact choice of this subset.

We wish to utilize three different observables to obtain our constraints: the overall optical depth τ to a source at redshift $z_{\rm s}$, the differential optical depth as a function of angular separation, and the differential optical depth as a function of lens redshift. Unfortunately, the last of these tests is uncertain due to possible incompleteness of the survey; higher-redshift lenses are more difficult to

[1] Multiple lens deflectors obviously make different predictions from single galaxies, and produce larger angular separations of images. We are interested in splittings due to single elliptical galaxies only.

Table 1. 13 lensing events from the 'CLASS statistical sample' of 8958 objects (adopted from Browne et al. (2003); see also Chae (2003)). 'ID' denotes identification of the lens – whether it is a spiral galaxy (s), an elliptical (e) or unknown (?); three lenses consist of multiple galaxies (m).

Survey	Lens	z_l	z_s	θ	ID	References
JVAS	B0218+357	0.68	0.96	0.33	s	Patnaik et al. (1993)
CLASS	B0445+123	0.56	–	1.33	?	Argo et al. (2003)
CLASS	B0631+519	–	–	1.16	?	Browne et al. (2003)
CLASS	B0712+472	0.41	1.34	1.27	e	Jackson et al. (1998)
CLASS	B0850+054	0.59	–	0.68	?	Biggs et al. (2003)
CLASS	B1152+199	0.44	1.01	1.56	?	Myers et al. (1999)
CLASS	B1359+154	–	3.21	1.65	?, m	Myers et al. (1999)
JVAS	B1422+231	0.34	3.62	1.28	e	Patnaik et al. (1992b)
CLASS	B1608+656	0.64	1.39	2.08	e, m	Myers et al. (1995)
CLASS	B1933+503	0.76	2.62	1.17	e	Sykes et al. (1998)
CLASS	B2045+265	0.87	1.28	1.86	?	Fassnacht et al. (1999)
JVAS	B2114+022	0.32/0.59	–	2.57	e, m	Augusto et al. (2001)
CLASS	B2319+051	0.62/0.59	–	1.36	e	Rusin et al. (2001)

measure due to their lower fluxes, while the source redshifts are more easily measurable for objects very far away (mainly quasars) and very close (mainly galaxies), and not those at intermediate distances. Because of these uncertainties, and because the redshift test does not add much to our constraints, we decide not to use the redshift-distribution test.[2]

We are therefore left with two tests: the total optical depth (τ test) and angular separation ($\mathrm{d}\tau/\mathrm{d}\theta$ test). The former test gives stronger constraints in both SIS and GNFW cases. The latter test, in the SIS case, is independent of z_s as long as $z_s \gtrsim 0.2$; henceforth, knowledge of z_s is not necessary and all single ellipticals (chosen as explained above) can be used for this test. In the GNFW case, knowledge of z_s is required for this test, and when it is not available we use the mean redshift of the measured sources, $z_s = 2$. (We have checked that the results change negligibly if, instead of $z_s = 2$, we use the histogram of the source distribution from Marlow et al. (2000), which is centred at $z_s = 1.27$ and has long tails.) Finally, we use the maximum lens separation $\theta_{\max}$ as an estimator of the angular separation θ. Although this estimator has been widely used in the literature due to the fact that $\theta_{\max}$ are readily available, we warn that the angle corresponding to the average image radius fitted to a lens model, for example, would be a better estimator. Nevertheless, we do not expect that using $\theta_{\max}$ will significantly bias the results, given the limited current statistics. Moreover, as higher σ_* roughly corresponds to larger angular separations, our results may only be biased to *higher* σ_*, strengthening our conclusion that this parameter is smaller than previously quoted in the literature.

In order to compute the *expected* optical depth for any given model, it is crucial to know the redshifts of source quasars and galaxies. The redshift distribution of JVAS/CLASS source objects has been discussed by Marlow et al. (2000), who spectroscopically followed up 42 sources at the William Herschel Telescope. Most of these sources are quasars; with a significant admixture of galaxies at $z \lesssim 1$. The mean redshift of this subsample is $\langle z_s \rangle = 1.27$ with a rms spread of 0.95. In this work, we use the full histogram distribution of the observed subsample of sources (figure 2 in Marlow et al. 2000), and assume that the redshift distribution of the subsample gives a good representation of the overall redshift distribution. We have to be cautious, however, because the lensed sources come from a fainter population than those in Marlow et al. (2000), and may be at different redshifts. The validity of this assumption has been examined by Chae (2003), who has reviewed existing observations and has found that the redshift distribution is expected not to change much at lower flux densities, corresponding to lensed sources.

Finally, we will need to know a few other details regarding the CLASS sample. The survey is complete at image separations $0.3 < \theta < 15$ arcsec (Helbig 2000; Myers et al. 2003). All confirmed JVAS/CLASS lenses have image separations $\theta < 3$ arcsec. The distribution of sources as a function of the total flux density S is well described by the power law

$$\frac{\mathrm{d}n}{\mathrm{d}S} \propto S^{-\eta} \tag{1}$$

where $\mathrm{d}n$ is the number of sources observed in the flux density interval $\mathrm{d}S$. For JVAS/CLASS, $\eta \simeq 2.1$ (Rusin & Tegmark 2001).

3 DENSITY PROFILE

There is good evidence that the density profiles of dark haloes on cluster scales depend on the halo mass (Keeton 1998; Wyithe et al. 2001; Li & Ostriker 2002). For the less massive haloes ($M \lesssim 10^{13}$ $\mathrm{M}_\odot$), SIS profiles are found to be adequate, while for large-mass haloes ($M \gtrsim 10^{13}$ $\mathrm{M}_\odot$) NFW profiles provide a good fit. This result is also expected from semi-analytical models, which show that objects smaller than $M_c \approx 10^{13}$ $\mathrm{M}_\odot$ are subject to baryonic cooling, whereby baryons collapse to the centre thereby enormously increasing the central density and lensing cross-section, and converting the shallow NFW profiles into the steep SIS (Rix et al. 1997; Kochanek & White 2001; Keeton 2001).

Galaxy clusters tend to lead to large lens separations and/or extended arcs and arclets. Because

$$\theta = 1.271\ \mathrm{arcmin} \frac{D_{ls}}{D_s} \left(\frac{M}{10^{15}\, h^{-1}\, \mathrm{M}_\odot} \right)^{2/3} \left(\frac{\rho_{\mathrm{crit}}}{\rho_{\mathrm{crit},0}} \right)^{1/3} \tag{2}$$

[2] Nevertheless, we have checked that the results of the redshift-distribution test agree with those of the other two tests. Furthermore, for the SIS case the quantity $(1/\tau)\ (\mathrm{d}\tau/\mathrm{d}z_l)$ is independent of galaxy parameters, and we have used it to check that the constraint on Ω_M and w is consistent with the adopted cosmological model $\Omega_M = 0.3$ and $w = -1$.

(Li & Ostriker 2002) where all quantities except $\rho_{\mathrm{crit},0}$ are evaluated at $z = z_{\mathrm{l}}$, we see that $M \gtrsim 10^{13}\ \mathrm{M}_{\odot}$ corresponds to $\theta \gtrsim 3$ arcsec. If we are interested primarily in lensing by individual galaxies rather than clusters, we should concentrate on image separations substantially smaller than this value. In the CLASS, all lensing events have separations smaller than 3 arcsec. We therefore conclude that the CLASS lenses are due to individual galaxies and not clusters.

Furthermore, we assume smooth, spherically symmetric density profiles. This assumption is widely used, and supported by the findings that the subclumps do not greatly affect the total optical depth for lensing (Flores, Maller & Primack 1996) and that asphericity of density profiles affects mostly the ratio of quads to doubles and not the optical depth (Rusin & Tegmark 2001).

Our goal in this paper is twofold. First, we would like to constrain the galaxy velocity dispersion *assuming* the SIS profile. The SIS profile has repeatedly been used in the past to constrain cosmological parameters, assuming the Schechter function parameters and the galaxy velocity dispersion to be known. We would like to reverse this process and see whether the previously-used σ_* is still favoured now that we have good knowledge of cosmological parameters.

Secondly, we would like to constrain the density profile of elliptical galaxies. As argued above, only the inner parts of lens galaxies (a few tens of kiloparsecs from the centre) are responsible for CLASS events. Moreover, as discussed in Section 7, there is good evidence that cores of galaxies are small and can safely be ignored. Therefore, it seems justified to adopt $\rho(r) \propto r^{-\beta}$ and to try to constrain β. We do this via the GNFW profile, as described in Section 7.

4 MODELLING THE LENS: SIS PROFILE

4.1 Number density of lenses

As we are interested in elliptical galaxies, we adopt the Schechter luminosity function (Schechter 1976) which has repeatedly been shown to be a good fit to the measurements[3]

$$\frac{\mathrm{d}\phi}{\mathrm{d}L}(L)\,\mathrm{d}L = \phi_* \left(\frac{L}{L_*}\right)^{\alpha} \exp(-L/L_*)\frac{\mathrm{d}L}{L_*}. \tag{3}$$

There has been much discussion as to what values of ϕ_* and α best describe the actual luminosity function. Typically, it is argued that $\phi_{*,\mathrm{TOT}} = 1.4 \times 10^{-2}\ h^3\ \mathrm{Mpc}^{-3}$ for all galaxies, of which $\approx$30 per cent are ellipticals (Postman & Geller 1984), so that $\phi_*^{\mathrm{ellip}} = 0.6 \times 10^{-2}\ h^3\ \mathrm{Mpc}^{-3}$; furthermore, $\alpha \approx -1$ with fairly large uncertainties. Recently, the SDSS (Blanton et al. 2001) claimed a more accurate determination of the local ($z \lesssim 0.2$) luminosity function: $\alpha = -1.20 \pm 0.03$ and $\phi_{*,\mathrm{TOT}} = (1.46 \pm 0.12) \times 10^{-2}\ h^3\ \mathrm{Mpc}^{-3}$.

To relate the luminosities to velocity dispersions, we use the Faber–Jackson relation (Faber & Jackson 1976)

$$\left(\frac{L}{L_*}\right) = \left(\frac{\sigma}{\sigma_*}\right)^{\gamma} \tag{4}$$

where it is typically assumed that $\gamma \approx 4$ for the SIS profile. Our principal goal is to determine the parameters ϕ_*, α, γ and σ_*.

[3] In order to compute optical depths for generalized dark matter distributions on cluster scales, many authors have assumed the Press–Schechter mass function (Press & Schechter 1974). As we are interested in constraining observational properties of elliptical galaxies, and because the lens identification from the CLASS indicates that most lenses are due to individual galaxies, for our purposes the Schechter luminosity function is more relevant.

4.2 Optical depth

The optical depth for a lens at redshift z_{l} due to a particular source at z_{s} is given by

$$\tau = \int_0^{z_{\mathrm{s}}} \mathrm{d}z_{\mathrm{l}} \frac{\mathrm{d}D_{\mathrm{l}}}{\mathrm{d}z_{\mathrm{l}}}(1+z_{\mathrm{l}})^3 \times \int_0^{\infty} \mathrm{d}L \frac{\mathrm{d}\phi}{\mathrm{d}L}(L)\sigma_{\mathrm{SIS}}(L, z_{\mathrm{l}}, z_{\mathrm{s}})B(L, z_{\mathrm{l}}, z_{\mathrm{s}}) \tag{5}$$

where ϕ is the comoving number density of lenses, L is their luminosity and σ_{SIS} $(L, z_{\mathrm{l}}, z_{\mathrm{s}})$ is their cross-section for lensing. $B(L, z_{\mathrm{l}}, z_{\mathrm{s}})$ is the magnification bias, describing the fact that lensed galaxies will be magnified, and therefore seen more easily, and therefore are enhanced in any flux limited survey. In equation (5) we have allowed for a general redshift and luminosity dependence of the number density, cross-section and magnification. For redshift-independent (as we first assume) ϕ_*, α and γ, $\mathrm{d}\phi/\mathrm{d}L$ depends only on L. Similarly, assuming that CLASS lenses are described by an SIS profile and the radio luminosity function is a power law, B is simply a constant (see below).

The density profile for the SIS is given by

$$\rho(r) = \frac{\sigma^2}{2\pi G r^2} \tag{6}$$

where σ is the velocity dispersion of the galaxy. This distribution produces an image separation of $2\theta_{\mathrm{E}}$, where the Einstein radius $\theta_{\mathrm{E}} = 4\pi(\sigma/c)^2 D_{\mathrm{ls}}/D_{\mathrm{s}}$, and D_{ls} and D_{s} are the angular diameter distances between the lens and source and the observer and source, respectively. The cross-section for lensing is therefore

$$\sigma_{\mathrm{SIS}} = \pi(\theta_{\mathrm{E}} D_{\mathrm{l}})^2 = 16\pi^3 \left(\frac{\sigma}{c}\right)^4 \left(\frac{D_{\mathrm{l}} D_{\mathrm{ls}}}{D_{\mathrm{s}}}\right)^2. \tag{7}$$

We only consider angular separations greater than some minimum value θ_{min}, because the resolution limit of the CLASS is $\theta_{\mathrm{min}} = 0.3$ arcsec, and multiple images with smaller separation angles than θ_{min} will not be resolved. The correspondence between the luminosity and angular separation for an SIS lens is

$$L = \left(\frac{\theta D_{\mathrm{s}} c^2}{8\pi D_{\mathrm{ls}} \sigma_*^2}\right)^{\gamma/2} L_* \tag{8}$$

where c is the speed of light, so that θ_{min} corresponds to some L_{min} as the lower limit of integration in equation (5).

We also need to compute the magnification bias, which is given by

$$B = \left(\int \frac{\mathrm{d}n}{\mathrm{d}S}\frac{S}{\mu}P(\mu)\mu^{-1}\,\mathrm{d}\mu\right)\left(\frac{\mathrm{d}n}{\mathrm{d}S}\right)^{-1} \tag{9}$$

where $\mathrm{d}n/\mathrm{d}S$ is the source luminosity function and $P(\mu)$ is the distribution of total magnifications. For the power-law luminosity function of the CLASS (cf. equation 1) and the distributions of magnifications for SIS lenses ($P(\mu) = 8\mu^{-3}$), the bias simplifies to (Sarbu et al. 2001)

$$B(L, z_{\mathrm{l}}, z_{\mathrm{s}}) = 4.76. \tag{10}$$

Finally, we are interested in the quantity $\mathrm{d}\tau/\mathrm{d}\theta$. This is given by

$$\left.\frac{\mathrm{d}\tau}{\mathrm{d}\theta}\right|_{\theta_1} = \left.\frac{\mathrm{d}\tau}{\mathrm{d}L}\right|_{L(\theta_1)} \times \left.\frac{\mathrm{d}L}{\mathrm{d}\theta}\right|_{\theta_1} = \int_0^{z_{\mathrm{s}}} \frac{\mathrm{d}D_{\mathrm{l}}}{\mathrm{d}z}(z_{\mathrm{l}})\,\mathrm{d}z_{\mathrm{l}}(1+z_{\mathrm{l}})^3 \frac{\mathrm{d}\phi}{\mathrm{d}L}(L, z_{\mathrm{l}}) \times \sigma_{\mathrm{SIS}}(L, z_{\mathrm{l}}, z_{\mathrm{s}})B(L, z_{\mathrm{l}}, z_{\mathrm{s}}) \times \left.\frac{\mathrm{d}L}{\mathrm{d}\theta}\right|_{\theta_1}, \tag{11}$$

and the correspondence between L and θ is given by equation (8). Note also that we have allowed, in these formulae, for a general dependence of the luminosity function, L, on z_l, which we consider later in this paper.

4.3 Dependence on parameters

To illustrate the dependence of our observables (τ and $\mathrm{d}\tau/\mathrm{d}\theta$) upon the parameters, we assume for a moment the following fiducial values: $\phi_* = 0.6 \times 10^{-2}\ h^3\ \mathrm{Mpc}^{-3}$, $\alpha = -1$, $\gamma = 4$ and $\sigma_* = 180\ \mathrm{km\ s}^{-1}$. For the purposes of this illustration, we have also assumed all sources to be at a fixed redshift, chosen to be $z_s = 1.3$.

The dependence of lensing statistics on the galaxy parameters and various degeneracies between these parameters have been investigated extensively in the literature (see, for example, Kochanek 1993a,b); here we present a brief overview. The variation of the total optical depth τ around this fiducial model can easily be computed to be

$$\begin{aligned}\mathrm{d}\ln\tau &= 2.07\,\mathrm{d}\ln z_s + 1.00\,\mathrm{d}\ln\phi_* + 0.69\,\mathrm{d}\ln\alpha + 4.16\,\mathrm{d}\ln\sigma_* \\ &\quad + 0.69\,\mathrm{d}\ln\gamma - 0.61\,\mathrm{d}\ln\Omega_\mathrm{M} + 0.61\,\mathrm{d}\ln w. \qquad (12)\end{aligned}$$

Perhaps not surprisingly, the strongest dependence is on the velocity dispersion, which strongly affects the lensing cross-section, as well as the luminosity function. ϕ_* enters linearly, and is degenerate with other factors, for example the magnification bias which is also a pure constant in the SIS case. Note, however, the much weaker dependence upon the cosmological parameters Ω_M and w. This reinforces the notion, independent of observational uncertainties, that lensing constraints might most effectively be used to constrain galaxy profile and luminosity function parameters, in particular σ_*, rather than cosmological parameters.

Fig. 1 shows the dependence of τ and $(1/\tau)\,(\mathrm{d}\tau/\mathrm{d}\theta)$ on σ_*. As expected, τ is a strongly increasing function of σ_*, while $(1/\tau)\,(\mathrm{d}\tau/\mathrm{d}\theta)$ favours higher angular splittings with increasing σ_*. As we shall describe, the fact that we only compare theory with observation for $\theta > 0.3$ arcsec (the angular resolution of the survey) allows the likelihood function for angular splitting to be consistent with that for optical depth, which favours models with low σ_*.

We briefly comment on the dependence on other parameters. Assuming $\phi_* = $ const, only τ depends on this quantity (we show in Section 9 that this is essentially true even if ϕ_* is redshift-dependent). Because τ scales directly with ϕ_*, the presence of other parameters implies that constraints on ϕ_* will be very weak. Furthermore, it is clear that, in the SIS case, τ only depends on the combination $\alpha + 4/\gamma$ (this is slightly spoiled by the fact that the luminosity integral starts at $L_\mathrm{min} > 0$). We have found that even trying to constrain this combination gives weak constraints – from either the τ test or the $\mathrm{d}\tau/\mathrm{d}\theta$ test. The only parameter that we are able to significantly constrain is σ_*.

5 THE LIKELIHOOD FUNCTION

As we have mentioned, there are several ways to use statistics of strong gravitational lensing. The total number of lenses – predicted versus observed – is an obvious and most commonly used statistics which provides information about the integrated optical depth for lensing. The angular splitting and redshift distribution of lenses are the other statistical observables, and in this work we use the former. We choose not to use the redshift distribution due to selection effects that are presumed to be significant in this test. Nevertheless, we have checked that the redshift distribution, if included, adds results consistent with the other two constraints.

The probability of the total optical depth can be computed using the Poisson distribution (e.g. Kochanek 1993b)

$$\mathcal{L}_\tau = \frac{N^x \exp(-N)}{x!} \qquad (13)$$

where x is the number of adopted lenses in the CLASS, $N = 8958\tau$ is the number of galaxies predicted by the model, and $\tau(\phi_*, \sigma_*, \alpha\ \gamma)$ is the computed optical depth given the Schechter function and cosmological parameters. This formula gives the correct likelihood for any value of τ. Recall that our determination of τ was based on the subsample redshift distribution of Marlow et al. (2000).

The likelihood for the angular distribution of galaxies is

$$\mathcal{L}_{\mathrm{d}\tau/\mathrm{d}\theta} = \prod_{i=1}^{M} \frac{1}{\tau_i}\left.\frac{\mathrm{d}\tau}{\mathrm{d}\theta}\right|_{\theta_i}, \qquad (14)$$

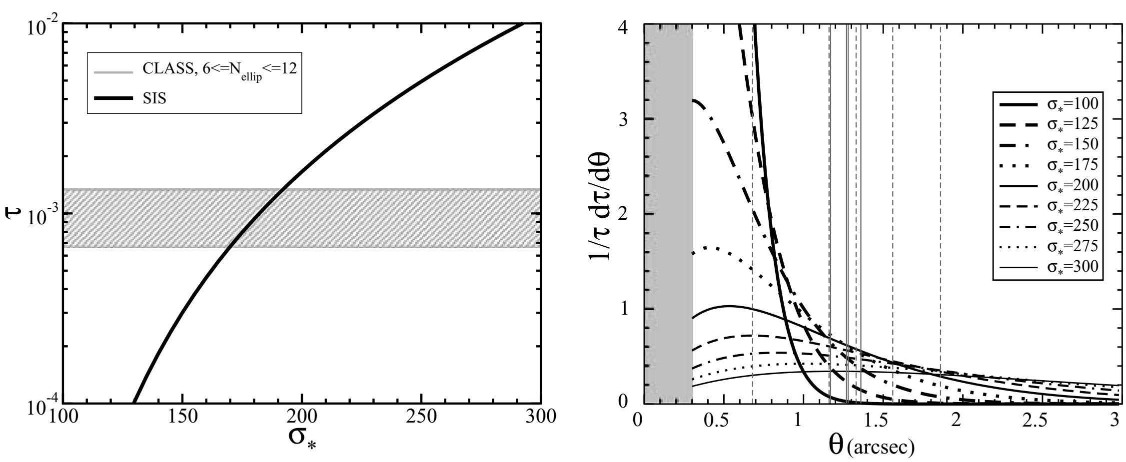

Figure 1. Dependence of the observables on the velocity dispersion σ_* (in km s^{-1}), assuming that all other parameters take their fiducial values. Left panel: The dependence of τ (the shaded region is the measured value from the CLASS, assuming the number of ellipticals to be between 6 and 12). Right panel: The dependence of $(1/\tau)\,(\mathrm{d}\tau/\mathrm{d}\theta)$ (vertical lines denote measurements from the CLASS, solid lines denote confirmed ellipticals, while dashed lines denote galaxies whose type has not been identified). The other Schechter function and cosmological parameters were fixed to their fiducial values from Section 4.3. Note that the CLASS is complete for $\theta > 0.3$ arcsec; therefore, all predicted quantities, such as $\mathrm{d}\tau/\mathrm{d}\theta$ in the right panel, were compared to measurements only for $\theta > 0.3$ arcsec. The quantity $\mathrm{d}\tau/\mathrm{d}z_l$ is very weakly dependent on σ_* (and other Schechter function parameters) and is not shown.

where the product runs over M lenses which we want to use for this test (recall, we use alternatively $M = 4$ or $M = 9$, and obtain virtually identical results for the two cases).

Finally, the joint likelihood for the redshift and angular distribution of galaxies, which takes into account correlations between these two observables, is given by

$$\mathcal{L}_{\mathrm{d}^2\tau/\mathrm{d}z\mathrm{d}\theta} = \prod_{i=1}^{6} \frac{1}{\tau_i} \left. \frac{\mathrm{d}^2\tau}{\mathrm{d}z\mathrm{d}\theta} \right|_{z_1(i)\theta_i}. \tag{15}$$

As mentioned in Section 2, we do not quote results from this test due to uncertainties regarding the redshift completeness. We do illustrate the constraints it gives in the GNFW case to demonstrate that including this result would not change our conclusions.

The total likelihood we use is

$$\mathcal{L}_{\mathrm{TOT}} = \mathcal{L}_\tau \times \mathcal{L}_{\mathrm{d}\tau/\mathrm{d}\theta} \tag{16}$$

and it depends on cosmological parameters, as well as the Schechter function parameters ϕ_*, α, γ and σ_*.

Equation (12) suggests that, for the SIS profile, by far the strongest dependence amongst the various lensing statistics is on the velocity dispersion σ_*. We determine the likelihood of σ_* by marginalizing over the other parameters

$$\mathcal{L}(\sigma_*) = \int \mathcal{L}(\sigma_*, \phi_*, \alpha, \gamma)\, \mathrm{d}\phi_*\, \mathrm{d}\alpha\, \mathrm{d}\gamma \tag{17}$$

where $\mathcal{L}$ refers to any combination of the likelihood functions discussed above.

6 SIS PROFILE: RESULTS

As mentioned above, the strong dependence of the optical depth on the velocity dispersion σ_* implies that we might hope to obtain an interesting constraint on σ_* despite the relatively poor lensing statistics and degeneracies between lensing parameters. We marginalize over the other three relevant parameters, which we give top-hat (uniform) priors of $\phi_* \in [0.5, 1.5] \times 0.6 \times 10^{-2}\ h^3\ \mathrm{Mpc}^{-3}$, $\gamma \in [3.0, 4.0]$, $\alpha \in [-1.3, 0.7]$. These ranges are conservative, allowing the full spread of values reported in various recent measurements. We have also made sure to use intervals that are *symmetric* around the traditionally favoured values, although it turns out that the exact choice of intervals affects the results very weakly. For example, the SDSS, from its commissioning data (Blanton et al. 2001), indicates that $\alpha = -1.20 \pm 0.03$ and $\phi_{*,\mathrm{TOT}} = (1.46 \pm 0.12) \times 10^{-2}\ h^3\ \mathrm{Mpc}^{-3}$, while the Two Degree Field survey from their preliminary sample of 45 000 galaxies (Cross et al. 2001) gives $\alpha = -1.09 \pm 0.03$ and $\phi_{*,\mathrm{TOT}} = (2.02 \pm 0.02) \times 10^{-2}\ h^3\ \mathrm{Mpc}^{-3}$; both of these quote the *total* luminosity function. Kochanek et al. (2001), on the other hand, isolated early-type galaxies from the K-band luminosity function, obtaining $\alpha = -0.92 \pm 0.10$ and $\phi_* = (0.45 \pm 0.06) \times 10^{-2}\ h^3\ \mathrm{Mpc}^{-3}$. Finally, there are direct, independent constraints on the Faber–Jackson slope γ from the lens data; for example, Rusin et al. (2003) find $\gamma = 3.29 \pm 0.58$ for early-type galaxies.

Fig. 2 shows the 68 and 95 per cent CL constraints from the τ and $\mathrm{d}\tau/\mathrm{d}\theta$ tests (top panels), as well as the constraints from the two tests combined (bottom panel). These constraints correspond to solid curves in the three panels; for comparison, the dashed line in the first panel shows the effect of fixing ϕ_*, α and γ to their 'fiducial' values, while the dashed lines in the top right and bottom panel indicate the effect of including the galaxies that are not identified as ellipticals in the angular separation test. First of all, note that the two independent tests are in remarkable agreement, and that both constrain σ_* quite strongly. The τ test gives $156 \leqslant \sigma_* \leqslant 226\ \mathrm{km\ s^{-1}}$ (at the 95 per cent CL), while the $\mathrm{d}\tau/\mathrm{d}\theta$ test gives $128 \leqslant \sigma_* \leqslant 272\ \mathrm{km\ s^{-1}}$ (95 per cent CL). Moreover, the $\mathrm{d}\tau/\mathrm{d}\theta$ results are roughly independent of the subsample of ellipticals we use, although the results are less tight in the baseline case when only the four 'secure' ellipticals are used; see Fig. 2. The two tests combined give $158 \leqslant \sigma_* \leqslant 220\ \mathrm{km\ s^{-1}}$ (95 per cent CL). Therefore, the overall favoured value of σ_* is actually smaller than the fiducial value of 225 km s^{-1} that has often been used to set constraints on cosmological parameters (Kochanek 1995, 1996; Falco, Kochanek & Muñoz 1998; Waga & Miceli 1999; Cooray et al. 1999), and, not surprisingly, is in agreement with the value used in studies that tended to favour non-zero Λ (Cheng & Krauss 1999; Chiba & Yoshii 1999). Note, however, that $\sigma_* \approx 225\ \mathrm{km\ s^{-1}}$ has also been obtained using the direct observations of early-type lens galaxies; for example, Koopmans & Treu (2003) obtain $\sigma_* \approx (225 \pm 15)\ \mathrm{km\ s^{-1}}$. Our results disfavour this result as representing a fiducial value.

We have found that the constraint on σ_* is very weakly dependent on the exact value of intervals allowed for other parameters. Furthermore, we find that independent constraints on other parameters of interest (ϕ_*, α and γ) are very weak, as expected from equation (12) and the fact that these parameters are highly correlated (e.g. α and γ). Finally, we have checked that the dependence of these results on cosmology is extremely weak; for example, marginalizing over the plausible values of the matter density $\Omega_{\mathrm{M}} \in [0.15, 0.40]$ (while maintaining the flatness condition) produces likelihoods that are only slightly broader.

7 MODELLING THE LENS: GNFW PROFILE

There is good evidence that galaxies have cuspy inner profiles. The strongest argument comes from N-body simulations, which argue for a profile $\rho(r) \propto r^{-\beta}$ with $\beta \simeq 1$ (Navarro, Frenk & White 1996, 1997) or perhaps $\beta \simeq 1.5$ (Moore et al. 1999; Ghigna et al. 2001) – in either case, a relatively steep profile. Another argument in favour of strongly cusped central profiles is given by the absence of central images in the CLASS; assuming $\rho(r) \propto r^{-\beta}$, $\beta > 1.8$ is obtained at 95 per cent CL (Rusin & Ma 2001). Finally, direct modelling of the observed lenses favours steep inner cusps with profiles close to isothermal: $\rho(r) \propto r^{-2}$ (Muñoz, Kochanek & Keeton 2001; Cohn et al. 2001; Treu & Koopmans 2002; Winn, Rusin & Kochanek 2003). These and other lines of evidence suggest that the central profiles of lens galaxies are steep and that cores, if they exist, are tiny, with radii of a few tens or hundreds of parsecs at most. Such small cores would not affect the lensing observables appreciably (Hinshaw & Krauss 1987).

To attempt to constrain the detailed profiles of elliptical galaxies, we must move beyond the simple SIS model. In order to explore the dependence of lensing statistics on the details of the density profile, we adopt the GNFW profile described below.

7.1 The GNFW profile

The GNFW profile (Zhao 1996) is given by

$$\rho(r) = \frac{\rho_{\mathrm{s}}}{(r/r_{\mathrm{s}})^\beta [1 + (r/r_{\mathrm{s}})]^{3-\beta}} \tag{18}$$

where r_{s} is the characteristic scale where the density profile shape can change. Because the integral of this density profile diverges at infinity, the mass of the halo is defined to be the mass contained within the radius r_{200} at which the density is 200 times greater than

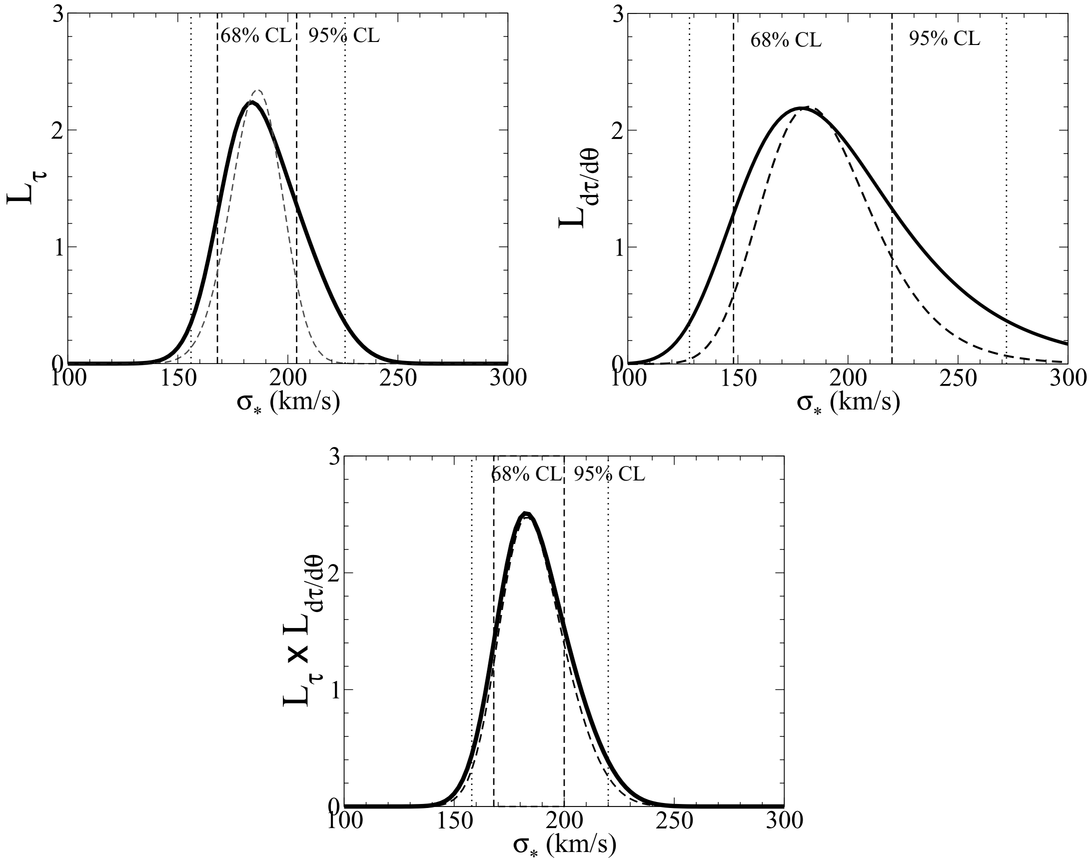

Figure 2. Constraints on the velocity dispersion σ_* assuming the SIS lens profile and marginalizing over the other luminosity function parameters. Top left: constraint from the τ test (for comparison, the dashed line denotes the case when the galaxy parameters have been fixed to their fiducial values of $\phi_* = 0.6 \times 10^{-2}\, h^3$ Mpc^{-3}, $\gamma = 4.0$ and $\alpha = -1.0$). Top right: constraint from the $\mathrm{d}\tau/\mathrm{d}\theta$ test, assuming four events that are due to ellipticals (solid line) and an additional five events that are due to unidentified galaxies (dashed line). Bottom: the two tests combined (the two curves refer to the two subsamples used in the $\mathrm{d}\tau/\mathrm{d}\theta$ test). Our baseline results, which we quote and to which the confidence regions correspond, refer to solid curves in the three panels.

the critical density of the universe *at that redshift*:

$$M \equiv M_{200} = 200 \left(\frac{4\pi}{3} r_{200}^3(z) \rho_c(z) \right). \tag{19}$$

The expression for the mass can further be written as

$$M = 4\pi \int_0^{r_{200}(z)} \rho r^2 \, \mathrm{d}r = 4\pi \rho_s(z) r_s^3(z) f(c(z)) \tag{20}$$

where

$$f(c) \equiv \int_0^c \frac{x^2 \, \mathrm{d}x}{x^\beta (1+x)^{3-\beta}}. \tag{21}$$

and the concentration parameter is defined as

$$c(z) \equiv \frac{r_{200}(z)}{r_s(z)}. \tag{22}$$

From equations (19)–(22) it follows that

$$r_s(z) = \frac{1}{c(z)} \left(\frac{3 M_{200}}{800 \pi \rho_c(z)} \right)^{1/3} \tag{23}$$

$$\rho_s(z) = \frac{200}{3} \rho_c(z) \frac{c(z)^3}{f(c(z))}. \tag{24}$$

Thus, the GNFW profile is determined by the choice of the inner density slope β and the concentration $c(z)$. Starting with these two parameters, we can compute $\rho_s(z)$ from equation (24) and then, given the mass of the halo, $r_s(z)$ from equation (23). Note that the GNFW profile for $\beta = 2$ and the SIS profile are different for three reasons: (1) the GNFW profile parameters are explicitly redshift-dependent; (2) the two profiles have different normalizations; and (3) the GNFW profile has a turnover at $r = r_s$, while the SIS does not.

7.2 The halo concentration

The halo concentration factor $c(z)$ is fortunately fairly well constrained due to recent results obtained using *N*-body simulations (e.g. Bullock et al. 2001a; Wechsler et al. 2002). For a pure NFW profile, the concentration of the haloes is well described by

$$c(z) = \frac{c_0}{(1+z)} \left(\frac{M}{M_*} \right)^{-0.13} \tag{25}$$

with $c_0 = 9$ and $M_* = 1.5 \times 10^{13}\, \mathrm{M}_\odot$ (the above papers actually quote results for $c_{\mathrm{vir}} \equiv r_{\mathrm{vir}}/r_s$ with r_{vir} being a virial radius, but the formula we quote accounts for the difference in definition quite accurately). The dependence on M is small and does not change the results much, while the dependence on redshift is important and fairly well understood (Wechsler et al. 2002). It is also important to account for the variance in c which occurs not only because of uncertainties in halo modelling, but also because of the variance in halo properties. We adopt an uncertainty in $\log_{10} c_0$ to be 0.14 (Bullock

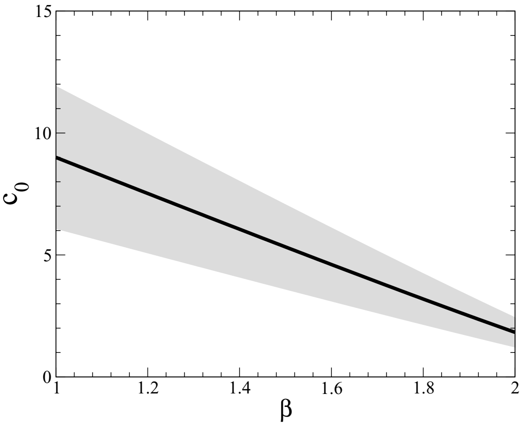

Figure 3. The mean value of the concentration parameter as a function of the inner slope of the density profile β (solid line). The value at $\beta = 1$ and its 1-σ uncertainty were obtained from N-body simulations. Concentration for other values of β was obtained by a simple recipe mentioned in the text, and adopting the same uncertainty in $\log_{10} c_0$.

et al. 2001a; Wechsler et al. 2002). Therefore, when computing the likelihood function we weight excursions around the middle value of c_0 by a Gaussian factor with this standard deviation.

Finally, we use the recipe from Li & Ostriker (2002) to compute c_0 for a GNFW profile given c_0 for a pure NFW; we assume that the ratio $r_{1/2}/r_{200}$ is independent of the density profile slope, where $r_{1/2}$ is defined as $M(r < r_{1/2}) = 1/2 M(r < r_{200})$. We retain the redshift and mass dependence of a GNFW profile as indicated in equation (25), as well as the same uncertainty in $\log_{10} c_0$. Fig. 3 shows the mean value of the parameter c_0 and its standard deviation, both as a function of β.

7.3 Cross-section for the GNFW profile

Lensing by GNFW haloes has been thoroughly explored by Wyithe et al. (2001) and Li & Ostriker (2002), and here we recapitulate the main results. The lens equation for a spherical symmetric lens is (Schneider, Ehlers & Falco 1993)

$$\boldsymbol{\beta} = \boldsymbol{\theta} - \boldsymbol{\alpha}(\boldsymbol{\theta}) \frac{D_{\mathrm{ls}}}{D_{\mathrm{s}}} \tag{26}$$

where $\boldsymbol{\beta}$ is the angular location of the source, $\boldsymbol{\theta}$ is the angular location of the lens, and $\boldsymbol{\alpha}$ is the deflection angle.[4] D_{ls} and D_{s} are the angular diameter distances between the lens and source and the observer and source, respectively. We define $\boldsymbol{\xi}$ and $\boldsymbol{\eta}$ to be the position vectors in the lens and source planes, respectively, and $x \equiv \xi/r_{\mathrm{s}}$ and $y \equiv (\eta/r_{\mathrm{s}})(D_{\mathrm{l}}/D_{\mathrm{s}})$, where D_{l} is the angular diameter distance to the lensing object. Then the surface mass density is given by

$$\Sigma(x) = 2\rho_{\mathrm{s}} r_{\mathrm{s}} \int_0^{\infty} (x^2 + z^2)^{-\beta/2} \left((x^2 + z^2)^{1/2} + 1\right)^{-3+\beta} \mathrm{d}z \tag{27}$$

and the mass by

$$M(x) = 2\pi r_{\mathrm{s}}^2 \int_0^x x' \Sigma(x') \, \mathrm{d}x'. \tag{28}$$

[4] The α and β used in this subsection are not to be confused with the Schechter function parameter α and the GNFW profile slope β used in the rest of the paper. Furthermore, note that σ_{GNFW} is the cross-section, while σ and σ_* refer to the galaxy velocity dispersion.

The deflection angle for a spherically symmetric source is

$$\alpha(x) = \frac{4GM(x)}{c^2 r_{\mathrm{s}} x}. \tag{29}$$

The lens equation then becomes

$$y = x - \mu_{\mathrm{s}} \frac{g(x)}{x} \tag{30}$$

where

$$g(x) \equiv \frac{M(x)}{4\pi \rho_{\mathrm{s}} r_{\mathrm{s}}^3} \tag{31}$$

$$\mu_{\mathrm{s}} \equiv \frac{4\rho_{\mathrm{s}} r_{\mathrm{s}}}{\Sigma_{\mathrm{crit}}} \tag{32}$$

$$\Sigma_{\mathrm{crit}} \equiv \frac{c_{\mathrm{light}}^2}{4\pi G} \frac{D_{\mathrm{s}}}{D_{\mathrm{l}} D_{\mathrm{ls}}}, \tag{33}$$

and c_{light} is the speed of light (to be distinguished from the concentration). Multiple images occur for x between $\pm x_{\mathrm{c}}$, where x_{c} is the solution of $\mathrm{d}y/\mathrm{d}x = 0$. Thus, the cross-section for the GNFW lens is

$$\sigma_{\mathrm{GNFW}} = \pi [y(x_{\mathrm{c}}) r_{\mathrm{s}}]^2. \tag{34}$$

7.4 GNFW optical depth for lensing

The optical depth for the GNFW lens is completely specified by properties of the lens, β and $c(z)$, the locations of the lens and source, z_{l} and z_{s}, and the cosmological abundance of the lenses. As in the SIS case, we use the Schechter luminosity function to model the number density of galaxies, together with the Faber–Jackson relation. The optical depth has the same form as in the SIS case:

$$\tau(z_{\mathrm{s}}) = \int_0^{z_{\mathrm{s}}} \mathrm{d}z_{\mathrm{l}} \frac{\mathrm{d}D_{\mathrm{l}}}{\mathrm{d}z_{\mathrm{l}}} (1 + z_{\mathrm{l}})^3 \times \int_0^{\infty} \mathrm{d}L \frac{\mathrm{d}\phi}{\mathrm{d}L}(L, z_{\mathrm{l}}) \sigma_{\mathrm{GNFW}}(z_{\mathrm{l}}, L) B(z_{\mathrm{l}}, z_{\mathrm{s}}, L). \tag{35}$$

In order to relate the optical depth to the parameters of a Schechter luminosity function, it is typical to define a one-dimensional dispersion velocity of a GNFW profile in analogy to that defined for an SIS galaxy:

$$\sigma^2 = \frac{GM}{2r_{200}}. \tag{36}$$

Combined with equation (19), this gives the mass as a function of the dispersion velocity

$$M = \frac{\sigma^3}{G} \sqrt{\frac{3}{100\pi G \rho_{\mathrm{c}}}}. \tag{37}$$

This mass then determines r_{s}

$$r_{\mathrm{s}}(z) = \frac{1}{c(z)} \frac{\sqrt{2}}{10} \frac{\sigma}{H(z)} \tag{38}$$

which, together with $\rho_{\mathrm{s}}(z)$ (equation 24), specifies μ_{s} (equation 32), which is necessary for the lensing equation.

Finally, we need the magnification bias for the GNFW haloes. For the source objects with the power-law flux distribution, as is the case with the CLASS, this is given by (Li & Ostriker 2002)

$$B = \frac{2}{3 - \beta} A_{\mathrm{m}}^{\beta - 1} \tag{39}$$

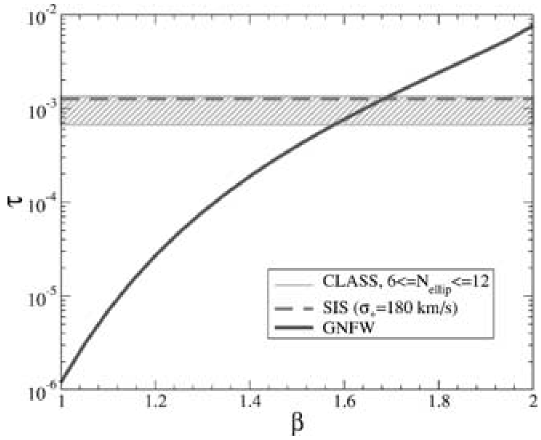

Figure 4. Optical depth versus the value of the inner density slope, β (rising solid line) for the fiducial values of Schechter function parameters from Section 4.3. Also shown is the value predicted by SIS profile (horizontal dashed line). The optical depth inferred from the CLASS is shown with the shaded region.

where

$$A_{\mathrm{m}} = \frac{2x_0}{y(x_{\mathrm{c}})y'(x_0)}. \tag{40}$$

where prime denotes the derivative with respect to x and and x_0 is defined by

$$y(x_0) = 0. \tag{41}$$

Equation (40) has been adopted from Oguri et al. (2002); magnification bias defined in this way agrees very well with ray-tracing simulations (C.-P. Ma, private communication). The magnification bias for GNFW haloes is very large, of the order a few tens or hundreds.

8 GNFW PROFILE: RESULTS

8.1 Dependence on β

To compute lensing statistics using the GNFW profile, we need to supply $c(z)$ and β. Our main goal here is to *determine* the inner density profile β, which is a parameter of considerable interest and to which the lensing statistics are very sensitive. Therefore, we marginalize over the concentration normalization c_0 and parameters of the Schechter luminosity function.

Fig. 4 shows the total optical depth of a GNFW lens as a function of β for $1 \leqslant \beta \leqslant 2$ and fiducial values of all other parameters. Also shown is the value predicted by the SIS model (horizontal dashed line), also with fiducial values of other parameters, as well as the optical depth actually measured by the CLASS (shaded region). (As remarked before, there is no reason why the GNFW profile at $\beta = 2$ should match the SIS profile case.) From this figure it is clear that the optical depth is a strong function of β. Note too that the lensing cross-section for $\beta > 2$ is formally infinite, although it becomes finite if we consider configurations in which both images are detectable. While values $\beta > 2$ are allowed by our analysis, they are disfavoured, and for computational reasons we only consider values $\beta \leqslant 2$.

8.2 Parameter choices

Our goal is to constrain the density profile β. We therefore have to consider how to include a host of other parameters. We adopt the concentration function $c(z)$ from N-body simulations, using equation (25) and choose c_0 with a Gaussian prior as discussed previously. We also need to marginalize over four luminosity function parameters (ϕ_*, σ_*, α and γ). We choose the same ranges for α, γ and ϕ_* as in the SIS case (see Section 6), plus a uniform prior $\sigma_* \in [150, 220]$ km s^{-1}, which is indicated by our SIS results. Remarkably, we find that interesting constraints on β are possible despite marginalizing over this large parameter space. As before, we assume the concordance cosmology ($\Omega_{\mathrm{M}} = 1 - \Omega_{\mathrm{DE}} = 0.3$; $w = -1$).

8.3 Constraints on β

The resulting constraints on the inner slope of the density profile are shown in Fig. 5. First, note that the total optical depth and angular separation tests (top panels) are in good agreement. The two tests together, when the likelihood function is marginalized over other parameters, yield the constraint $1.64 \leqslant \beta \leqslant 1.92$ at the 68 per cent CL and $1.50 \leqslant \beta \leqslant 2.00$ at the 95 per cent CL (bottom-left panel). As in the SIS case, these results are insensitive to the exact ranges allowed for the luminosity function parameters. Moreover, we have checked that the angular separation test is insensitive to the choice of lens data, i.e. whether we use the four single deflectors confirmed to be ellipticals, or all nine single deflectors that are not identified as spirals. To be conservative, all results we quote correspond to the former choice and are represented by solid lines in Fig. 5 (for more on this choice, see Section 2). We also show the likelihood for the angular and redshift test combined using the *three* elliptical lenses with complete redshift and angular separation information ($(1/\tau)(\mathrm{d}^2\tau/\mathrm{d}z_l\,\mathrm{d}\theta)$; bottom-right panel), which we did not use in the analysis due to uncertain systematic effects in the selection of lens redshifts. It is clear that the combined angular and redshift test is consistent with the other tests, and combining it with the τ test would further strengthen the final constraint on β, as shown with the dotted curve in the bottom-left panel.

Although the favoured slope is significantly steeper that the canonical NFW $\rho \propto r^{-1}$ profile, it is expected that the shallow NFW profiles seen in simulations become steeper due to baryonic infall (e.g. Kochanek & White 2001). The results of our analysis are in excellent agreement with such a scenario. Furthermore, these constraints are in good agreement with direct modelling of the observed lenses (Muñoz et al. 2001; Cohn et al. 2001; Treu & Koopmans 2002; Winn et al. 2003) which typically favours a steep, near-isothermal cusp. Finally, the results are insensitive to the exact values of cosmological parameters; for example, marginalizing over the plausible values of the matter density $\Omega_{\mathrm{M}} \in [0.15, 0.40]$ produces negligible increase of the width of our contours.

We can also constrain the GNFW concentration parameter $c(z)$ and the density profile slope β jointly. In Fig. 6 we display the N-body determination of the concentration parameter as a function of β, and overlay this with our lensing constraint on c_0 versus β, using the τ test. For any given β, we allow c_0 to be a free parameter, and retain the redshift and mass dependence of $c(z)$ as in equation (25). Not surprisingly, the allowed value of β reported above coincides with the overlap region between the N-body result and our lensing constraint. Note, however, that lensing imposes constraints on the concentration that are independent of N-body results. In particular, if the galaxies indeed have pure NFW ($\beta = 1$) profile, lensing statistics implies that the concentration parameter c_0 has to be greater than 15, which is in conflict with the results of N-body simulations.

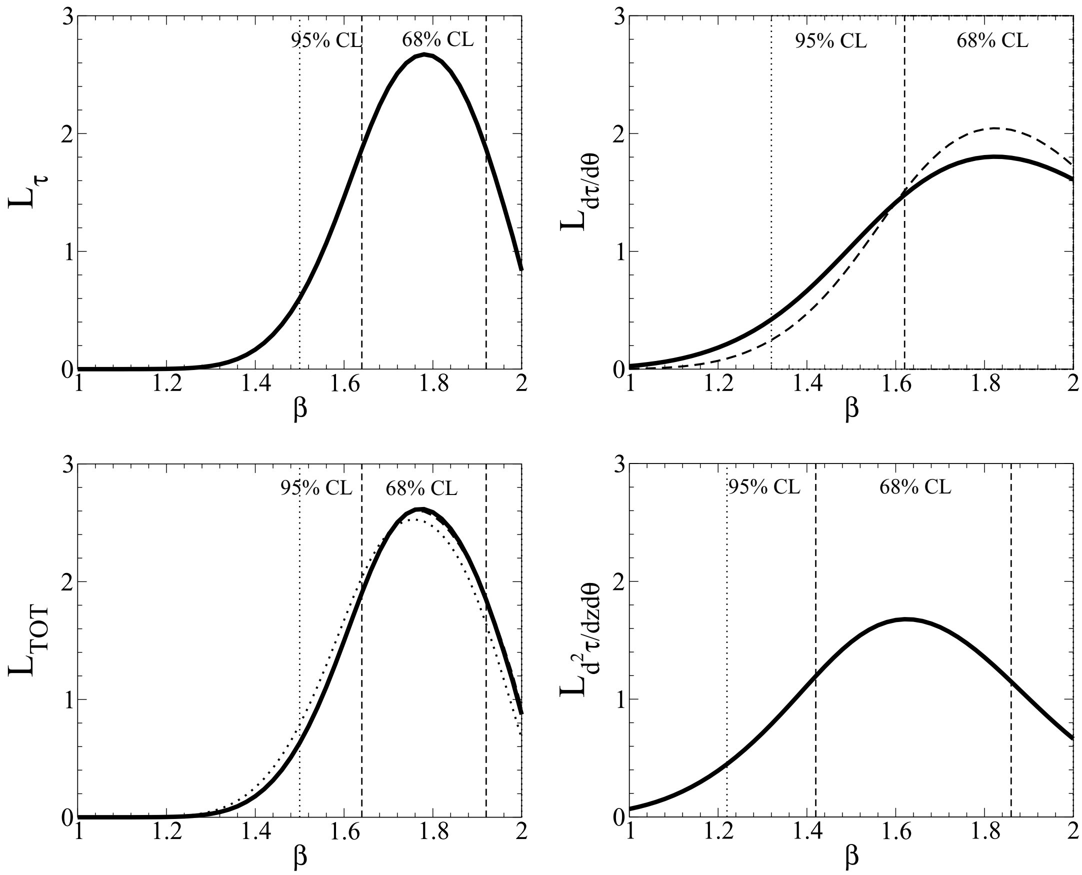

Figure 5. Constraints on the inner density slope β, marginalized over all other relevant parameters. The likelihood functions are shown for τ and $(1/\tau)(\mathrm{d}\tau/\mathrm{d}\theta)$ (top panels), as well as for the two combined (lower-left panel). The lower-right panel shows the likelihood for the angular and redshift test combined ($(1/\tau)(\mathrm{d}^2\tau/\mathrm{d}z_l\,\mathrm{d}\theta)$), which we did not use in the analysis due to the uncertain redshift selection function, but show here to illustrate that it is consistent with the other tests. For the likelihoods using the angular separation test, we show the results assuming four single deflectors confirmed to be ellipticals (solid lines), and, alternatively, all nine single deflectors that are not identified as spirals (dashed lines). Note that the solid and dashed lines in the combined likelihood test essentially overlap. The dotted line in the combined likelihood test shows the likelihood when τ and $(1/\tau)(\mathrm{d}^2\tau/\mathrm{d}z_l\,\mathrm{d}\theta)$ tests are combined.

9 REDSHIFT DEPENDENCE OF THE LUMINOSITY FUNCTION?

We mentioned previously that one of the great difficulties with using gravitational lensing statistics as a probe is that the parameters that describe the abundance of galaxies can depend on redshift. (In the GNFW case, the concentration parameter $c(z)$ is allowed to vary with redshift, as predicted by numerical simulations.) To make progress, essentially all authors in the past who wanted to use lensing statistics assumed that these functions were redshift-independent. In particular, it is expected that the number density ϕ_* and the characteristic velocity dispersion σ_* may be strongly dependent on redshift due to galaxy accretion and mergers.[5]

Direct constraints on the redshift dependence of the luminosity and abundance of galaxies are still crude, made difficult by poor statistics and a variety of systematic effects. Even rough agreement between various surveys has not been achieved. For example, while the Canada–France Redshift Survey (CFRS; Lilly et al. 1995), the Canadian Network for Observational Cosmology 2 (CNOC2) survey (Lin et al. 1999) and the Calar Alto Deep Imaging Survey (CADIS) (Fried et al. 2001) all observe an increase of ϕ_* for early-type galaxies between redshifts of zero and $z \sim 1$, the Autofib survey (Ellis et al. 1996) and the numerical simulations by Nagamine et al. (2001) conclude just the opposite. It is clear that obtaining the redshift dependence of number densities and characteristic velocities per spectral type and their various covariances will take some time. Keeton (2002) has argued that a variation in ϕ_* with z can cancel out much of the cosmological sensitivity of lensing statistics. However, we note that this variation alone is probably unrealistic. At the same time, mergers and accretion will be expected to cause a variation σ_*, which will have the opposite effect of a variation in ϕ_* on lensing statistics, and indeed may overwhelm it. To accurately account for evolution, it is probably best to match on to N-body simulations of the galaxy mass function, which in fact suggest that the number density of galaxies with a specific value of σ_* is relatively constant with z (e.g. Bullock et al. 2001b).

To estimate the maximal possible effect of evolution (assuming an evolution in the galaxy number density only), we used an SIS profile, which simplifies calculations. If we then consider a number density dependence of galaxies as suggested by Lin et al. (1999)

$$\phi_*(z) = \phi_*(0)10^{0.4Pz} \tag{42}$$

[5] This situation is reminiscent of that in the analysis of galaxy surveys, where it is necessary to know the galaxy-to-mass bias in order to obtain the distribution of matter from the observed distribution of galaxies. In the past, most authors assumed the bias to be constant, while it is widely suspected that it depends on scale, redshift and galaxy type.

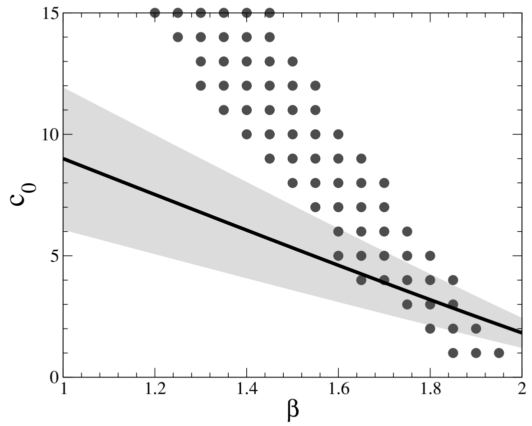

Figure 6. Same as Fig. 3, but overlapped with the 68 per cent CL constraint on β and c_0 from the τ test of lensing statistics (filled circles). We use the total optical depth for the latter constraint, and retain the redshift and mass dependence of $c(z)$ as in equation (25). Note that the region of overlap coincides roughly with the allowed range of these two parameters based on the likelihood function.

we can estimate how the results would change for non-zero values of P. For the τ test, the change is as expected; for example, for $P = 1$ the number density increases by $\sim$60 per cent (assuming the average lens redshift is $\sim$0.5), which corresponds to the decrease in the favoured σ_* by $\sim$10 per cent in order to preserve agreement with the measured τ, cf. equation (12). For the $(1/\tau)(\mathrm{d}\tau/\mathrm{d}\theta)$ test, the redshift dependence of ϕ_* largely cancels out in the numerator and denominator of this quantity. Therefore, as expected, the total optical depth is more sensitive to the redshift dependence of ϕ_*, while the angular distribution of lenses is not. Again, we expect that the actual impact of evolution will be much less severe than that discussed above, because mergers and accretion will tend to produce a variation in σ_* with z that will cancel the effect of the variation in ϕ_*.

10 CONCLUSIONS

The use of strong gravitational lensing statistics in order to probe cosmology has a long history. Nevertheless, the dominant uncertainty in the predictions of lensing statistics has to do with estimates of galaxy parameters, not cosmological ones. Because of the recent revolutions in observational cosmology that have allowed us to pin down the basic cosmological parameters with relatively good accuracy, gravitational lensing statistics now provide us with a new opportunity to probe the structure of galaxies and the trends of galaxy evolution. Our results represent a first step in this regard. Nevertheless, it is quite remarkable that, in spite of the paucity of lensing statistics at this time, we obtain non-trivial limits on galaxy properties. It is also significant that these limits are largely independent of cosmological uncertainties. Because we are primarily interested here in constraining observational galaxy parameters, we have used the Schechter luminosity function, which gives the number density of galaxies in terms of luminosity, rather than the mass function, which is more relevant for more massive haloes associated with clusters ($M \gtrsim 10^{13}$ M$_\odot$).

Assuming the SIS density profile, we find that the mean velocity dispersion for elliptical galaxies is small, with $168 < \sigma_* < 200$ km s^{-1} at 68 per cent CL, consistent with a number of earlier estimates used in lensing analyses (e.g. Chiba & Yoshii 1999; Cheng & Krauss 2001), but significantly smaller than the 'canonical' value of 225 km s^{-1} often quoted in the literature. Perhaps more significantly, assuming the GNFW density profile with inner slope $1 \leqslant \beta \leqslant 2$, we constrain β to be in the range $1.64 \leqslant \beta \leqslant 1.92$ at 68 per cent CL. This is definitely inconsistent with the $\beta = 1$ slope advocated by N-body simulations for the dark matter haloes profiles. Fig. 6 shows that a profile with $\beta = 1$ could produce the observed lensing statistics only with an unreasonably high concentration ($c_0 > 15$). At the same time, it is a well-known fact that N-body simulations do not include additional physics, e.g. the baryonic infall, that makes the inner profiles of haloes and galaxies steeper. Consequently, our result for the density slope is in good agreement with the expectations, as well as with similar analyses (e.g. Keeton 2001; Kochanek & White 2001; Rusin & Ma 2001) or direct modelling (Cohn et al. 2001; Treu & Koopmans 2002; Winn et al. 2003). The lack of high-separation events (>3 arcsec) in the JVAS/CLASS has been used to suggest that there are two populations of haloes in the universe (Keeton 1998; Li & Ostriker 2002): small-mass galaxy-size haloes with possibly steep density profiles ($\beta \sim 2$), and large-mass haloes with shallow density profiles ($\beta \sim 1$). The former correspond to the elliptical galaxies we are interested in here, and our results confirm that a steep slope seems to be required to explain these events.

There remain some issues that require further exploration. In particular, the total optical depth produces a likelihood function that tends to suggest a slope that is less steep than that favoured by exploring the redshift dependence and angular splitting of lensing events. This may be an artefact of our limited statistics, but it could also signal the need to consider a more complicated, perhaps two-component, galaxy distribution in order to consistently model lensing events.

Needless to say, the most significant factor not explicitly taken into account here is a possible redshift evolution of galaxy number density and velocity dispersion. Very little is known observationally about the evolution of these quantities beyond $z \sim 0.3$. As we have discussed in Section 9, there are reasons to believe that the effects of evolution will not significantly alter the allowed parameter ranges we have determined here.

Finally, we note that there is great potential to improve these constraints as better statistics are obtained using current and future observational efforts. In particule Deep Extragalactic Evolutionary Probe 2 (DEEP2) redshift survey (Davis et al. 2002) will provide a velocity function for galaxies at redshift $z \sim 1$, which will allow us to explore the evolution of galaxy parameters with redshift with a much higher sensitivity than currently available.

ACKNOWLEDGMENTS

We would like to thank Joanne Cohn, Marc Davis, Chuck Keeton, Chung-Pei Ma, Paul Schechter and Risa Wechsler for useful conversations, and the anonymous referee for numerous useful comments and suggestions. DH and LMK acknowledge the hospitality of the Kavli Institute for Theoretical Physics, where this work was completed. The work of the CWRU particle astrophysics group is supported by the Department of Energy.

REFERENCES

Argo M. K. et al., 2003, MNRAS, 338, 957
Augusto P. et al., 2001, MNRAS, 326, 1007
Biggs A. D. et al., 2003, MNRAS, 338, 1084
Blanton M. R. et al., 2001, ApJ, 121, 2358

Browne I. W. A. et al., 2003, MNRAS, 341, 13
Bullock J. S., Kolatt T. S., Sigad Y., Somerville R. S., Kravtsov A. V., Klypin A. A., Primack J. R., Dekel A., 2001a, MNRAS, 321, 559
Bullock J. S., Dekel A., Kolatt T. S., Primack J. R., Somerville R. S., 2001b, ApJ, 550, 21
Chae K.-H. et al., 2002, Phys. Rev. Lett., 89, 151301
Chae K.-H., 2003, MNRAS, in press (astro-ph/0211244)
Cheng Y.-C. N., Krauss L. M., 1999, Int. J. Mod. Phys. A., 15, 697 (2000)
Cheng Y.-C. N., Krauss L. M., 2001, NewA, 6, 249
Chiba M., Yoshii Y., 1999, ApJ, 510, 42
Cohn J. D., Kochanek C. S., McLeod B. A., Keeton C. R., 2001, ApJ, 554, 1216
Cooray A. R., Huterer D., 1999, ApJ, 513, L95
Cooray A. R., Quashnock J. M., Miller C. L., 1999, ApJ, 511, 562
Cross N. et al., 2001, MNRAS, 324, 825
Davis M. et al., 2002, preprint (astro-ph/0209419)
Ellis R. S., Colless M., Broadhurst T., Heyl J., Glazebrook K., 1996, MNRAS, 280, 235
Faber S. M., Jackson R. E., 1976, ApJ, 204, 668
Falco E. E., Kochanek C. S., Muñoz J. A., 1998, ApJ, 494, 47
Fassnacht C. D. et al., 1999, AJ, 117, 658
Flores R. A., Maller A. H., Primack J. R., 1996, ApJ, 535, 555
Fried J. W. et al., 2001, A&A, 367, 788
Fukugita M., Turner E. L., 1991, MNRAS, 253, 99
Fukugita M., Futamase T., Kasai M., Turner E. L., 1992, ApJ, 393, 3
Ghigna S., Moore B., Governato F., Lake G., Quinn T., Stadel J., 2001, ApJ, 544, 616
Helbig P., 2000, preprint (astro-ph/0008197)
Hinshaw G., Krauss L. M., 1987, ApJ, 320, 468
Im M., Griffiths R. E., Ratnatunga K., 1997, ApJ, 475, 457
Jackson N. et al., 1998, MNRAS, 296, 483
Keeton C. R., 1998, PhD thesis, Harvard Univ.
Keeton C. R., 2001, ApJ, 561, 46
Keeton C. R., 2002, ApJ, 575, L1
Keeton C. R., Madau P., 2001, ApJ, 549, L25
King L. J., Browne I. W. A., Marlow D. R., Patnaik A. R., Wilkinson P. N., 1999, MNRAS, 307, 225
Kochanek C. S., 1993a, MNRAS, 261, 453
Kochanek C. S., 1993b, ApJ, 419, 12
Kochanek C. S., 1995, ApJ, 453, 545
Kochanek C. S., 1996, ApJ, 466, 638
Kochanek C. S., White M., 2001, ApJ, 559, 531
Kochanek C. S. et al., 2001, ApJ, 560, 566
Koopmans L. V. E., Treu T., 2003, ApJ, 583, 606
Krauss L. M., 2000, Proceedings of Third International Conference on the Identification of Dark Matter, York, UK (astro-ph/0102305)
Krauss L. M., White M., 1992, ApJ, 394, 385
Li L. -X., Ostriker J. P., 2002, ApJ, 566, 652
Lilly S. J., Tresse L., Hammer F., Crampton D., Le Fevre O., 1995, ApJ, 455, 108
Lin H., Yee H. K. C., Carlberg R. G., Morris S. L., Sawicki M., Patton D. R., Wirth G., Shepherd C. W., 1999, ApJ, 518, 533
Marlow D. R., Rusin D., Jackson N. J., Wilkinson P. N., Browne I. W. A., Koopmans L., 2000, AJ, 119, 2629
Moore B., Quinn T., Governato F., Stadel J., Lake G., 1999, MNRAS, 310, 1147
Muñoz J. A., Kochanek C. S., Keeton C. R., 2001, ApJ, 558, 657
Myers S. T. et al., 1995, ApJ, 447, L5
Myers S. T. et al., 1999, AJ, 117, 2565
Myers S. T. et al., 2003, MNRAS, 341, 1
Nagamine K., Fukugita M., Cen R., Ostriker J. P., 2001, MNRAS, 327, L10
Navarro J. F., Frenk C. S., White S. D. M., 1996, ApJ, 462, 563
Navarro J. F., Frenk C. S., White S. D. M., 1997, ApJ, 490, 493
Oguri M., Taruya A., Suto Y., 2001, ApJ, 559, 572
Oguri M., Taruya A., Suto Y., Turner E. L., 2002, ApJ, 568, 488
Patnaik A. R., Browne I. W. A., Wilkinson P. N., Wrobel J. M., 1992a, MNRAS, 254, 655
Patnaik A. R., Browne I. W. A., Walsh D., Chaffee F. H., Foltz C. B., 1992b, MNRAS, 259, 1P
Patnaik A. R., Browne I. W. A., King L. J., Muxlow T. W. B., Walsh D., Wilkinson P. N., 1993, MNRAS, 261, 435
Porciani C., Madau P., 2000, ApJ, 532, 679
Postman M., Geller M. J., 1984, ApJ, 281, 95
Press W. H., Schechter P. L., 1974, ApJ, 187, 425
Rix H.-W., de Zeeuw P. T., Cretton N., van der Marel R. P., Carollo C. M., 1997, ApJ, 488, 702
Rusin D., Ma C.-P., 2001, ApJ, 549, L33
Rusin D. et al., 2001, AJ, 122, 591
Rusin D., Tegmark M., 2001, ApJ, 553, 709
Rusin D. et al., 2003, ApJ, 587, 143
Sarbu N., Rusin D., Ma C.-P., 2001, ApJ, 561, L147
Schechter P. L., 1976, ApJ, 203, 297
Schneider P., Ehlers J., Falco E. E., 1993, Gravitational Lenses. Springer, Berlin
Sykes C. M. et al., 1998, MNRAS, 301, 310
Takahashi R., Chiba T., 2001, ApJ, 563, 489
Treu T., Koopmans L. V. E., 2002, ApJ, 575, 87
Turner E. L., Ostriker J. P., Gott J. R., 1984, ApJ, 284, 1
Waga I., Miceli A. P. M. R., 1999, Phys. Rev. D, 59, 103507
Wechsler R. H., Bullock J. S., Primack J. R., Kravtsov A. V., Dekel A. R., 2002, ApJ, 568, 52
Winn J., Rusin J., Kochanek C. S., 2003, ApJ, 587, 80
Wyithe J. S. B., Turner E. L., Spergel D. N., 2001, ApJ, 555, 504
Zhao H. S., 1996, MNRAS, 278, 488

This paper has been typeset from a TEX/LATEX file prepared by the author.